Cell Reports

Report

A STAT3 protein complex required for mitochondrial mRNA stability and cancer

Graphical abstract

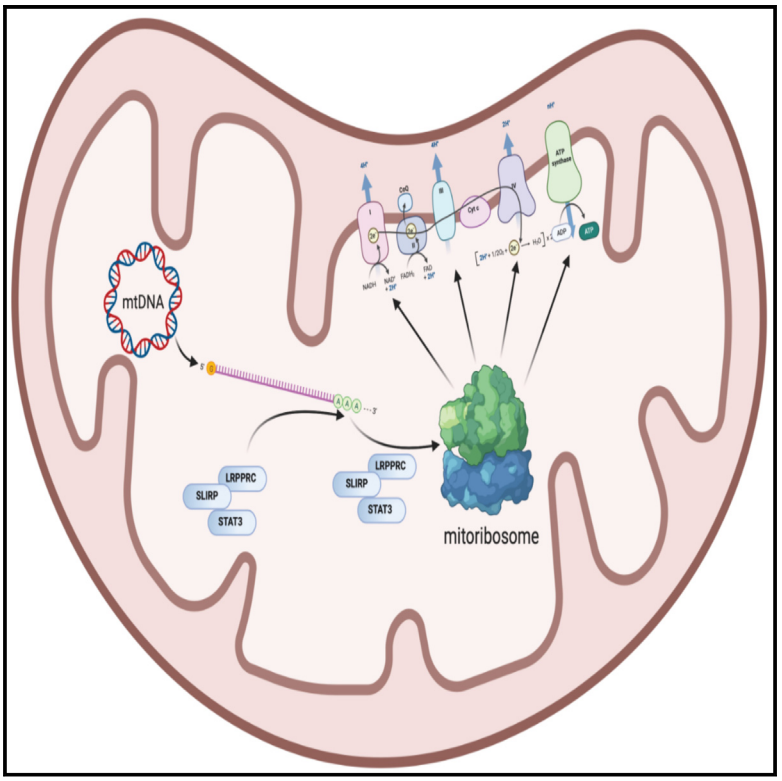

Highlights

- Unbiased MS shows that mitochondrial STAT3 binds to the LRPPRC-SLIRP complex
- STAT3 regulated mitochondrial mRNA stability, ribosomal delivery, and translation kinetics
- The STAT3-LRPPRC-SLIRP complex is enriched in LUAD patient tissue
- Blocking STAT3 binding to LRPPRC reduces tumor formation *in vivo*

Authors

C. Dilanka Fernando, W. Samantha N. Jayasekara, Chaitanya Inampudi, ..., Tracy M. Josephs, Daniel J. Garama, Daniel J. Gough

Correspondence

daniel.garama@hudson.org.au (D.J.G.), daniel.gough@hudson.org.au (D.J.G.)

In brief

Fernando et al. describe a STAT3-LRPPRC-SLIRP complex critical for the regulation of mitochondrial mRNA stability and translation kinetics. They show increased abundance of this complex in LUAD compared to adjacent healthy tissue, and the loss of this complex impedes tumor growth *in vivo*.

Fernando et al., 2023, Cell Reports *42*, 113033
September 26, 2023
https://doi.org/10.1016/j.celrep.2023.113033

CellPress

Cell Reports

CellPress
OPEN ACCESS

Report

A STAT3 protein complex required for mitochondrial mRNA stability and cancer

C. Dilanka Fernando,[1,2,12] W. Samantha N. Jayasekara,[1,2] Chaitanya Inampudi,[1,2] Maija R.J. Kohonen-Corish,[3,4,5,6] Wendy A. Cooper,[5,7,8] Traude H. Beilharz,[9] Tracy M. Josephs,[10,11] Daniel J. Garama,[1,2,12,*] and Daniel J. Gough[1,2,13,*]

[1]Department of Molecular Translational Science, Faculty of Medicine, Nursing and Health Sciences, Monash University, Clayton, VIC 3800, Australia
[2]Centre for Cancer Research, Hudson Institute of Medical Research, Clayton, VIC 3168, Australia
[3]Garvan Institute of Medical Research, Darlinghurst, NSW 2010, Australia
[4]Woolcock Institute of Medical Research, Glebe, NSW 2037, Australia
[5]School of Medicine, Western Sydney University, Campbelltown, NSW 2560, Australia
[6]Faculty of Science, UTS Sydney, Ultimo, NSW 2007, Australia
[7]Tissue Pathology and Diagnostic Oncology, NSW Health Pathology, Royal Prince Alfred Hospital, Missenden Road, Camperdown, NSW 2050, Australia
[8]Sydney Medical School, University of Sydney, Camperdown, NSW 2006, Australia
[9]Development and Stem Cells Program and the Department of Biochemistry and Molecular Biology, Biomedicine Discovery Institute, Monash University, Clayton, VIC 3800, Australia
[10]Drug Discovery Biology Theme, Monash Institute of Pharmaceutical Sciences, Monash University, Parkville, VIC 3052, Australia
[11]ARC Centre for Cryo-Electron Microscopy of Membrane Proteins, Monash Institute of Pharmaceutical Sciences, Monash University, Parkville, VIC 3052, Australia
[12]These authors contributed equally
[13]Lead contact
*Correspondence: daniel.garama@hudson.org.au (D.J.G.), daniel.gough@hudson.org.au (D.J.G.)
https://doi.org/10.1016/j.celrep.2023.113033

SUMMARY

Signal transducer and activator of transcription 3 (STAT3) is a potent transcription factor necessary for life whose activity is corrupted in diverse diseases, including cancer. STAT3 biology was presumed to be entirely dependent on its activity as a transcription factor until the discovery of a mitochondrial pool of STAT3, which is necessary for normal tissue function and tumorigenesis. However, the mechanism of this mitochondrial activity remained elusive. This study uses immunoprecipitation and mass spectrometry to identify a complex containing STAT3, leucine-rich pentatricopeptide repeat containing (LRPPRC), and SRA stem-loop-interacting RNA-binding protein (SLIRP) that is required for the stability of mature mitochondrially encoded mRNAs and transport to the mitochondrial ribosome. Moreover, we show that this complex is enriched in patients with lung adenocarcinoma and that its deletion inhibits the growth of lung cancer *in vivo*, providing therapeutic opportunities through the specific targeting of the mitochondrial activity of STAT3.

INTRODUCTION

Signal transducer and activator of transcription 3 (STAT3) is a latent transcription factor activated by tyrosine phosphorylation in response to a plethora of cytokines and growth factors to mediate cellular differentiation, proliferation, immune function, and metabolism.[1] Deregulation of STAT3 tyrosine phosphorylation, typically due to elevated cytokine secretion (e.g., interleukin-11 [IL-11] in gastric cancer[2]) or mutation in upstream tyrosine kinases (e.g., JAK2 in myeloproliferative disease[3]) drives the constitutive expression of pro-survival and proliferative genes. This augmented STAT3 activity is observed in approximately 50% of human cancers. STAT3 activity was exclusively attributed to its role as a nuclear transcription factor until recently, when a mitochondrial pool of STAT3 was identified[4,5] that is critical for tumor development and is independent of nuclear STAT3 activity.[4–6] Mitochondrial STAT3 augments the activity of the electron transfer chain (ETC)[4,5] and the production of reactive oxygen species (ROS)[7–9] and blocks the opening of the mitochondrial permeability transition pore (mPTP).[10] The mechanism of STAT3 mitochondrial activity has been proposed to be through its interaction with complex I of the ETC[5] and with cyclophilin D.[11] However, isobaric labeling mass spectrometry revealed a ratio of STAT3 to complex I of approximately 1:100,000,[12] making this physical interaction an implausible mechanism by which STAT3 regulates ETC activity. In this report, we identify a mechanism of STAT3 mitochondrial activity that has significant implications in cancer as well as in stem cell differentiation[13] and immune,[5,14] cardiac,[5] and neural[9] biology.

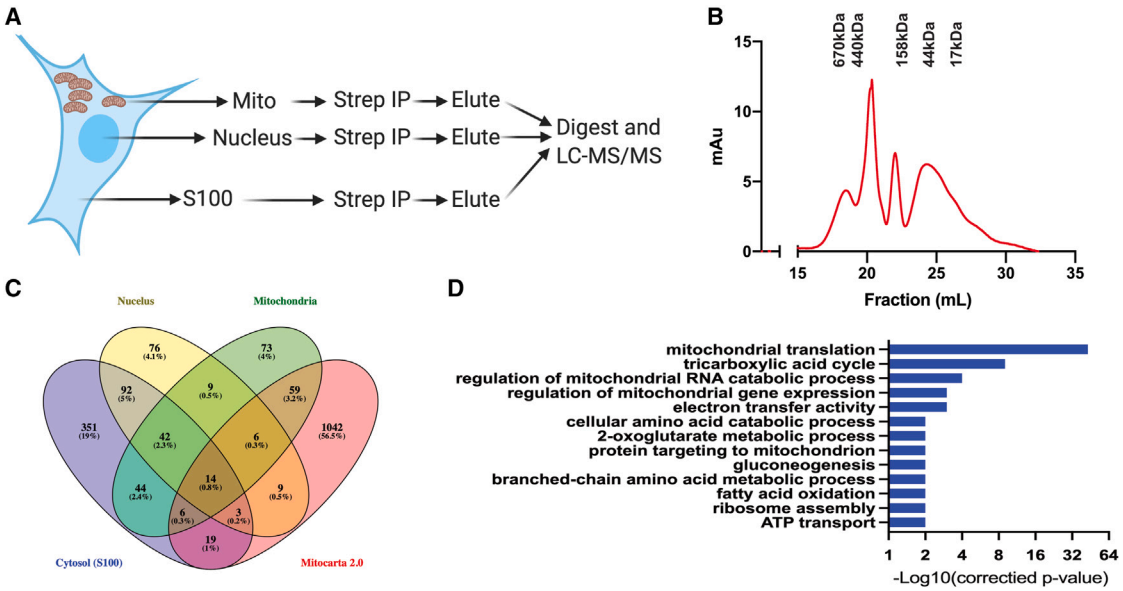

Figure 1. Mitochondrial STAT3 forms a complex with LRPPRC and SLIRP

(A) Schematic representation of IP-MS workflow.

(B) Size-exclusion chromatography of STAT3-containing complexes from isolated mitochondria. Molecular weight markers were separated in previous runs, and retention time corresponding to each indicated size is indicated.

(C) Venn diagram showing the overlap between STAT3-interacting proteins identified from A549 cytosolic, mitochondrial, and nuclear fractions and the mitochondrial proteome (Mitocarta 2.0).

(D) −Log10 p values of Gene Ontology analysis of mitochondrial STAT3-interacting proteins. Analysis performed with the ClueGO application for Cytoscape[15,16] with a pathway p value set at <0.001.

See related content in Figure S1 and Table S1.

RESULTS

Mitochondrial STAT3 forms a complex with LRPPRC and SLIRP

Despite the relative paucity of mitochondrial STAT3, its activity in this organelle is likely to be dependent on interaction with other mitochondrial proteins. Therefore, to identify the mitochondrial STAT3 interactome, we undertook an unbiased mass spectrometry approach. Due to the requirement of mitochondrial STAT3 for RAS-driven tumors,[4,6] endogenous STAT3 was deleted from the *KRAS* mutant A549 lung adenocarcinoma cell line, which was subsequently reconstituted with dual FLAG- and Strep-tagged STAT3 (Figure S1A). Cells were fractionated into cytosolic, nuclear, and mitochondrial compartments (Figures 1A and S1B), and STAT3, together with associated proteins, was isolated from each fraction using anti-FLAG or streptactin resin. To determine whether mitochondrial STAT3 exists in multimeric complexes, proteins were eluted from capture beads and separated by size-exclusion chromatography, which revealed that mitochondrial STAT3 predominantly exists in a ~400 kDa complex with minor species at ~670 and ~100 kDa; this latter peak is consistent with the known size of monomeric STAT3 (Figure 1B). Together, these data suggest that STAT3 forms multimeric complex(es) in the mitochondria.

The identities of STAT3-interacting proteins from each cellular compartment were determined by liquid chromatography-tandem mass spectrometry (LC-MS/MS) and prioritized for validation if the interacting protein(s) appeared in the Mitocarta database of mitochondrial proteins (Figure 1C).[17] Gene Ontology (GO) analysis of the 92 putative mitochondrial interacting proteins (Table S1) showed significant enrichment in mitochondrial RNA-catabolic processes ($p = 5.67 \times 10^{-5}$), mitochondrial translation ($p = 1.58 \times 10^{-43}$), and mitochondrial gene expression ($p = 6.21 \times 10^{-4}$) (Figure 1D). Two putative mitochondrial STAT3-interacting proteins common to these GO terms (leucine-rich pentatricopeptide repeat containing [LRPPRC] and SRA stem-loop-interacting RNA-binding protein [SLIRP]) form a known heterotetrameric protein complex at a 2:2 ratio[18] of 350–400 kDa.[19] The predicted size of an LRPPRC (158 kDa), SLIRP (12 kDa), and STAT3 (88 kDa) complex at a 2:2:1 ratio is consistent with mass of the major mitochondrial STAT3 species (~400 kDa) (Figure 1B). STAT3, LRPPRC, and SLIRP are not exclusively mitochondrial proteins, with pools present in mitochondria, cytosol, and nucleus.[1,20,21] Therefore, the interaction between endogenous STAT3, LRPPRC, and SLIRP within the mitochondria was shown by reciprocal immunoprecipitation (IP) of endogenous protein from isolated, pure mitochondrial fractions (Figures 2A–2C) and confirmed by proximity ligation assay (PLA) (Figures 2D and S2). While mitochondrial STAT3 is necessary for RAS transformation, STAT3 is also required for many other cancers with low incidence of RAS mutation, including gastric cancer.[22] The requirement for the mitochondrial activity of STAT3 in these cancers remains unclear. Therefore, to determine whether this complex was restricted to KRAS-transformed cells, reciprocal IP of endogenous STAT3, LRPPRC, and SLIRP from the mitochondria was performed in the RAS wild-type,

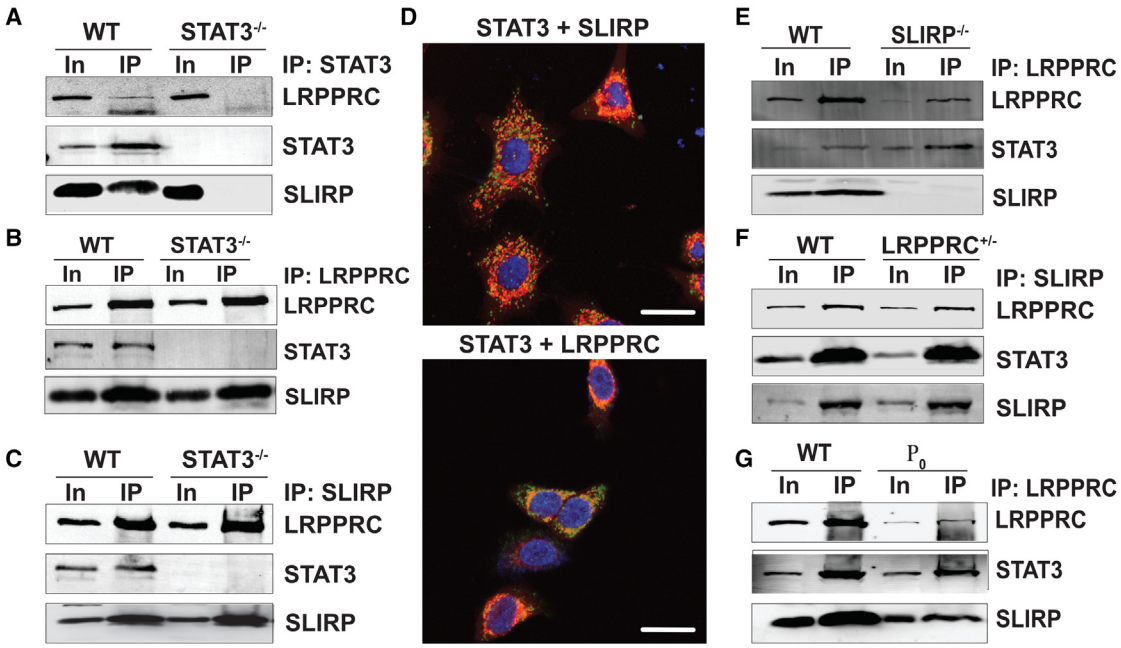

Figure 2. STAT3 interacts with LRPPRC and SLIRP independent of RNA

(A–C) Immunoprecipitation of mitochondrial fractions from A549 WT or *STAT3*$^{-/-}$ cells with antibodies against (A) STAT3, (B) LRPPRC, or (C) SLIRP and western blots probed with indicated antibodies.

(D) Proximity ligation assay using antibodies against either LRPPRC and STAT3 or SLIRP and STAT3 (green), counterstained with DAPI (blue) and MitoTracker (red). Scale bar: 20 μm.

(E and F) Mitochondrial fractions from (E) SLIRP knockout or (F) LRPPRC knockdown cells were immunoprecipitated with LRPPRC or SLIRP antibodies, respectively, and western blots probed with the indicated antibodies.

(G) LRPPRC immunoprecipitation from the mitochondrial fractions of matched A549 wild-type (WT) and A549 ρ_0 cells.

See related content in Figures S2, S4 and S5.

MKN28 gastric cancer cell line (Figure S3). Together, these data show that STAT3 forms a complex with LRPPRC and SLIRP in the mitochondria that is not restricted to KRAS mutant cells.

STAT3's association with the LRPPRC-SLIRP complex is independent of mitochondrial RNA

Mitochondria have a discrete circular genome that encodes 13 mRNA, 22 tRNA, and 2 rRNA sequences.[23] Each of the 13 mitochondrial mRNAs (mtRNA) encode proteins required for ETC activity. Transcription generates polycistronic precursor RNA transcripts, which are cleaved at the 5′ and 3′ ends by specific RNAse enzymes and undergo maturation including polyadenylation. mtRNA polyadenylation has the dual function of generating a stop codon and increasing mtRNA stability.[24,25] The SLIRP-LRPPRC complex binds to maturing mtRNA species and facilitates poly(A) tail elongation,[26] mtRNA stability[27] and transport to the mitochondrial ribosome for efficient translation.[28] The RNA-binding capacity of the complex is conferred by LRPPRC,[18] and the loss of either LRPPRC or SLIRP leads to the degradation of the remaining member of the complex.[18] A549 cells deficient in STAT3, LRPPRC, or SLIRP were generated by CRISPR-Cas9 (Figure S4A). LRPPRC is an essential protein[26,29]; therefore, heterozygote cell lines were generated, and the expected ~50% reduction in LRPPRC protein expression was confirmed (Figure S4B). STAT3 deletion had no impact on the steady-state abundance of either LRPPRC or SLIRP, indicating that these genes are not STAT3 transcriptional target genes (Figures 2A, 2B, and S4), nor does the loss of STAT3 alter complex formation or stability (Figures 2B and 2C). As expected, the complete loss of SLIRP results in degradation of LRPPRC but has no impact on STAT3 expression (Figure S4A). Likewise, the partial loss of LRPPRC concomitantly reduces SLIRP expression (Figure S4A). Reciprocal IP in cells lacking SLIRP reveals that STAT3 still interacts with LRPPRC, suggesting that the STAT3 interaction is mediated by LRPPRC, not SLIRP (Figure 2E). We do observe a STAT3-SLIRP interaction in LRPPRC knockdown cells (Figure 2F). However, in this latter case, it is possible that this is through the residual LRPPRC protein in these heterozygous cells.

The SLIRP-LRPPRC complex is stabilized by binding to mtRNA. Therefore, to determine whether the STAT3-LRPPRC-SLIRP interaction is dependent on RNA, A549-ρ_0 cells, which lack mitochondrial DNA and, therefore, mitochondrial RNA and ETC activity, were generated (Figure S5). Importantly, STAT3, LRPPRC, and SLIRP are nuclear-encoded genes that are unaffected by the deletion of the mitochondrial genome. Reciprocal IPs on mitochondria isolated from A549-ρ_0 cells show that the STAT3-LRPPRC and STAT3-SLIRP interactions are independent of mtRNA (Figure 2G). Together, these data show that while the LRPPRC-SLIRP complex is stabilized by the expression of SLIRP and the interaction with mtRNA, the association of STAT3 with this complex is independent of either SLIRP or RNA.

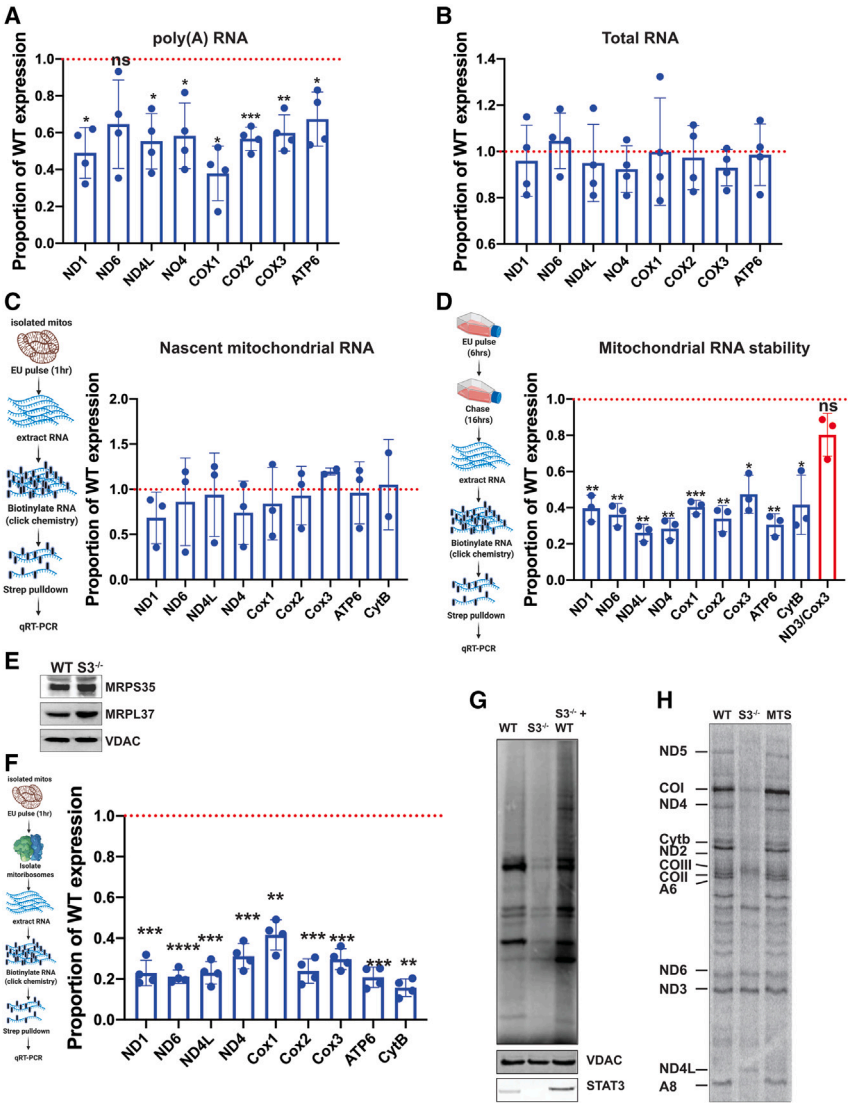

Figure 3. STAT3 is required for mature mitochondrial RNA stability and transport to the mitochondrial ribosome for efficient mitochondrial translation

(A and B) Total RNA was isolated from the mitochondria of A549 STAT3 WT or *STAT3*$^{-/-}$ cells and cDNA synthesized with (A) oligo(d-T) primers or (B) random hexamers. The abundance of each mtRNA species was determined by quantitative real-time PCR and plotted relative to that observed in WT cells. The red dotted line represents equivalent expression between genotypes.

(C) Nascent mitochondrial RNA was labeled with EU for 1 h prior to isolation and changes in the rate of mitochondrial transcription in the absence of STAT3 expression determined by qRT-PCR.

(D) STAT3 loss decreases mitochondrial RNA stability. EU pulse-chase in A549 STAT3 WT or *STAT3*$^{-/-}$ cells and the abundance of each mtRNA species determined by qRT-PCR, normalized to the expression of the nuclear housekeeping gene *β2M* and expressed relative to WT. Data represent the mean ± SD from at least three biological replicates. *p < 0.05, **p < 0.01, ***p < 0.001 (Student's t test). See related content in Figures S6 and S7. A549 STAT3 WT or *STAT3*$^{-/-}$ cells were pulsed with EU for 1 h, and mitochondrial ribosome fractions were isolated.

(E) Equivalent abundance of mitochondrial ribosomes in STAT3 WT and *STAT3*$^{-/-}$ cells was confirmed by western blot.

(F) RNA was biotinylated and isolated from mitochondrial ribosomal fractions and abundance of each mtRNA species at the mitochondrial ribosome determined by qRT-PCR and expressed relative to WT cells. All experiments were performed at least 3 times and plotted as the mean ± SD. Student's t test was used to determine significance. *p < 0.05, **p < 0.01, ***p < 0.001.

(G and H) A549 STAT3 WT or *STAT3*$^{-/-}$ cells (G) or ^{35}S labeling of mitochondrially encoded proteins (H) in Ras-transformed MEFs (STAT3 WT, *STAT3*$^{-/-}$, or *STAT3*$^{-/-}$ reconstituted with mitochondrially restricted STAT3 [MTS]).

STAT3 is required for the stability of mature mtRNA species

The function of the LRPPRC-SLIRP complex is to enable elongation of poly(A) tails, mtRNA stability, and transport to the ribosome. Therefore, the role for STAT3 in these functions was interrogated. Multiplex poly(A) test RNA sequencing (mPAT)[30] is a next-generation amplicon sequencing technology that captures the full 3′ endogenous poly(A) tail from candidate mRNA, enabling the determination of poly(A) tail length. mPAT analysis on matched STAT3 wild-type and null A549 cells revealed that STAT3 loss has no impact on mRNA poly(A) length of a panel of either mitochondrially encoded or nuclear-encoded mitochondrial genes (Figure S6). Whether STAT3 loss affected the expression of immature and mature, poly(A)-tailed mtRNA was determined by performing qRT-PCR on cDNA generated by either random hexamers (i.e., both immature and mature mtRNA) or oligo(d-T) primers (i.e., only the mature poly(A)-tailed mtRNA). STAT3 knockout resulted in a significant reduction in the poly(A)-tailed mtRNA species (Figure 3A); however, it had no impact on the expression of total mitochondrial RNA (Figure 3B). To ensure that this was not influenced by any impact of STAT3 on mitochondrial DNA copy number, the mitochondrial DNA content was determined in matched wild-type and *STAT*$^{-/-}$ A549 cells and showed that there is no significant STAT3 dependency (Figure S7). Together, these data confirm that STAT3 specifically influences the abundance of mature mtRNA species.

While our data show that STAT3 specifically impacts the abundance of mature poly(A), but not the total pool of mtRNA, it is important to note that STAT3 is a potent nuclear transcription factor and has been reported to bind to the mitochondrial transcription factor TFAM[31] and to mitochondrial DNA[32] and to regulate the transcription of the mitochondrial genome.[31] Therefore, to determine whether STAT3 regulates transcription of the mitochondrial genome, intact mitochondria isolated from STAT3 wild-type and knockout A549 cells were pulsed with 5-ethynyluridine (EU) for 1 h to label nascent mtRNA species. qRT-PCR on cDNA generated from captured EU-RNA revealed no significant difference in the abundance of newly synthesized mtRNA in

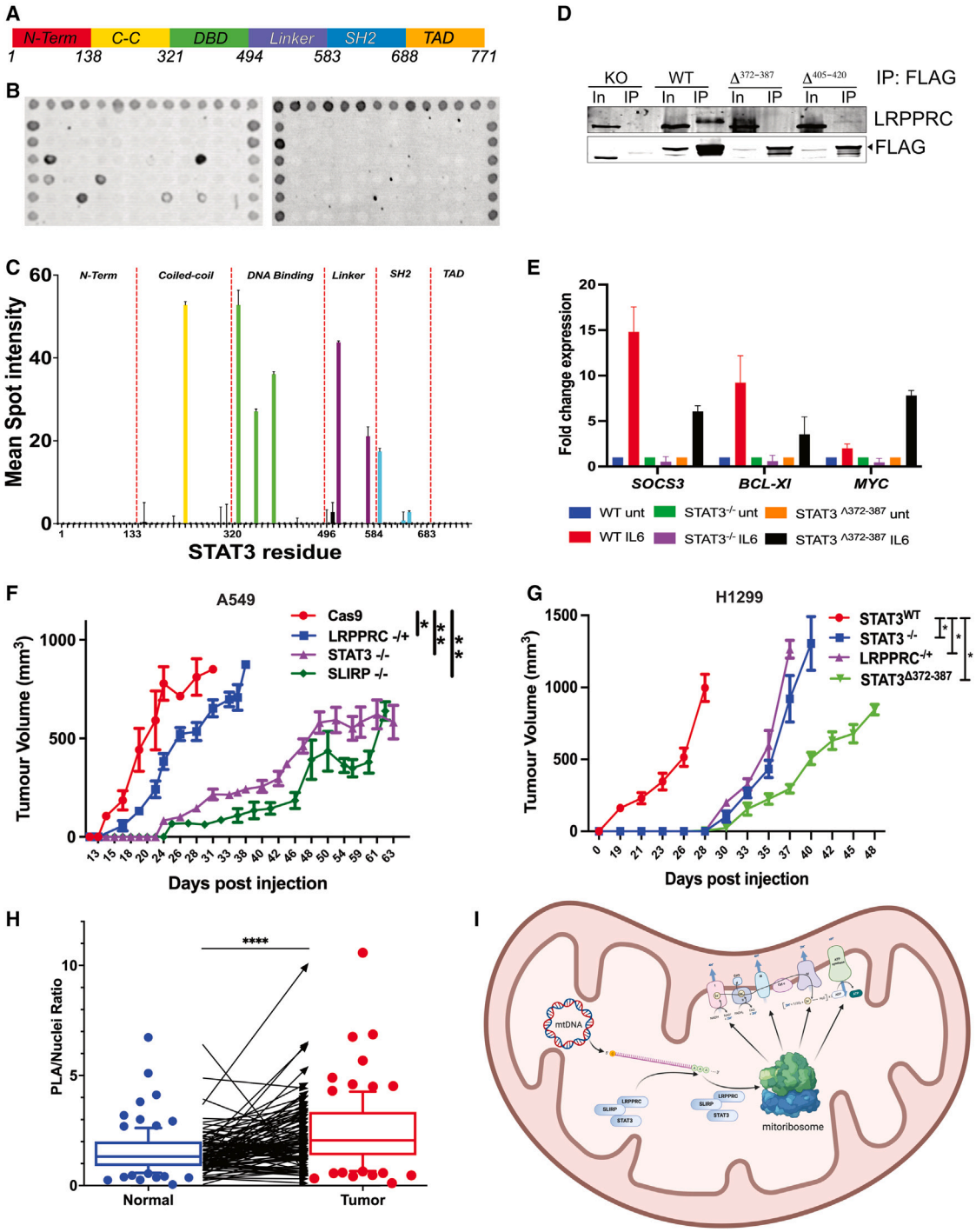

Figure 4. STAT3 interaction with the LRPPRC-SLIRP complex is required for tumor growth

(A) Schematic overview of STAT3 domains. C-C, coiled coil; DBD, DNA-binding domain; TAD, transcriptional activation domain.

(B) Spotted cellulose arrays were incubated with lysates from *STAT3*$^{-/-}$ (left panel) or *SLIRP*$^{-/-}$ (right panel) to enable LRPPRC complex to bind to STAT3 peptides. Complex interaction was detected by LRPPRC antibody. Border spots are for orientation.

(C) Spotted array analysis was performed three times and spot intensity calculated. Graph represents mean spot intensity ± SD for three independent experiments. The location of the first amino acid of each peptide sequence is shown on the x axis, dashed lines show the border of each STAT3 domain, and the bar color follows the schematic in (A).

(D) STAT3 was immunoprecipitated from mitochondria isolated from the indicated cell lines and the interaction between LRPPRC and STAT3 determined by western blot. Data are representative of at least three independent experiments.

(legend continued on next page)

the absence of STAT3 (Figure 3C). These data, together with those in Figure 3B, confirm that STAT3 is not acting as a mitochondrial transcription factor in this context. We therefore hypothesize that the reduction in mature mtRNA species in STAT3 knockout cells was due to decreased RNA stability. To test this, A549 and A549 *STAT3*$^{-/-}$ cells were pulsed with EU for 6 h and chased in fresh media for 16 h. EU-RNA was biotinylated and isolated, and the abundance of each mtRNA species was determined. During mtRNA maturation, the polycistronic RNA transcript is cleaved between adjacent genes. Therefore, as a control, a primer pair that generates an amplicon spanning the junction between *MT-ND3* and *MT-COX3*, which is abolished in mature mtRNA, was designed. A significant reduction in each of the mature mtRNA species was observed in the absence of STAT3, while the *MT-ND3/COX3* junctional amplicon was not significantly altered (Figure 3D). Therefore, STAT3 is specifically required for the stability of mature mtRNA species and has no impact on mitochondrial copy number, on mitochondrial transcription, or on the poly(A) tail length of mtRNA.

STAT3 loss blocks mtRNA transport to the mitochondrial ribosome and impedes mitochondrial translation

Mitochondria have their own discrete ribosome (mitoribosome) containing approximately 80 nuclear-encoded proteins that is more proteinaceous than its bacterial ancestor.[33] Loss of SLIRP results in impaired transport of mtRNA to the mitoribosomes.[28] In the absence of STAT3, the abundance of mitochondrial poly(A) mRNA species is diminished (Figure 3A); however, the abundance of newly synthesized mtRNA is unchanged (Figure 3C). Therefore, to assess the transport of mRNA to the mitoribosome without the influence of decreased mtRNA stability, mitochondria isolated from STAT3 wild-type and *STAT3*$^{-/-}$ cells were pulsed with EU for 1 h and mitoribosome purified. Protein and RNA were isolated from the mitoribosomal fraction, and western blot for protein constituents of the heavy (MRPL37) and light (MRPS35) ribosomal subunits confirmed that there is no STAT3-dependent defect in mitoribosomal protein abundance (Figure 3E). However, in the absence of STAT3, there was a significant decrease in the abundance of each newly synthesized, EU-pulsed mtRNA species at the mitoribosome (Figure 3F), indicating that STAT3 is required for the transport of newly synthesized mitochondrial RNA to the ribosome for translation. Indeed, ^{35}S pulse labeling of newly synthesized mitochondrial polypeptides in A549 wild-type and *STAT3*$^{-/-}$ cells revealed a significant defect in the synthesis of mitochondrially encoded proteins, which was restored by re-expression of STAT3 in *STAT3*$^{-/-}$ cells (Figure 3G). This deficit is specific to the mitochondrial encoded proteins, as there is no change in the expression of the nuclear-encoded mitochondrial protein voltage-dependent anion channel (VDAC). To ensure that the STAT3-dependent modulation of mitochondrial translation was dependent on the mitochondrial pool of STAT3, ^{35}S pulse-labeling experiments were performed on a panel of HRasV12-transformed mouse embryo fibroblasts (MEFs) that were *STAT3*$^{+/+}$ or *STAT3*$^{-/-}$ or that had been engineered to stably express an exclusively mitochondrially localized STAT3 mutant (mitochondrially restricted STAT3 [MTS]).[4] Similar to the observation in A549 cells, there was a significant defect in mitochondrial translation in the absence of STAT3 that was completely restored in MTS-STAT3-expressing cells (Figure 3H).

The STAT3 DNA-binding domain contains the LRPPRC interaction region

To define the region of STAT3 required for interaction with LRPPRC, we designed a spotted peptide array that consists of 15 amino acid linear polypeptides tiling across the entire STAT3 sequence with 4 amino acid overlap with the previous linear polypeptide. Peptides were immobilized on cellulose membrane and incubated with cell lysate from *STAT3*-deficient cells to avoid any STAT3-STAT3 interactions confounding interpretation. Membranes were washed and probed with an LRPPRC antibody to determine the regions of STAT3 that interact with LRPPRC (Figure 4B). As a control, membranes were incubated in the presence of lysate from *SLIRP*-deficient cells that, due to SLIRP loss, are also deficient in LRPPRC protein (Figure 2E). Seven STAT3 peptides consistently showed interaction with LRPPRC. In contrast, no immunoreactivity was observed on control membranes. These seven STAT3 peptides were found in the coiled-coil, DNA-binding, linker, and SH2 domains (Figures 4A–4C). To confirm the requirement of these STAT3 regions for the interaction with LRPPRC, we generated STAT3 mutants with the deletion of the identified 15 amino acid sequences that were stably expressed in *STAT3*$^{-/-}$ H1299 cells. IP revealed that the deletion of amino acids 372–387 resulted in the loss of LRPPRC interaction (Figure 4D). Amino acids 372–387 reside in the DNA-binding domain of STAT3 but do not directly bind to DNA (Figure S8). Therefore, to determine whether the deletion of this sequence alters STAT3's activity as a transcription factor, we treated STAT3 wild-type, *STAT3*$^{-/-}$, and STAT3$^{\Delta 372-387}$ cells with IL-6 for 16 h and measured the expression of the *bona fide* STAT3-target genes *SOCS*, *MYC*, and *BCL-XL* by quantitative real-time PCR. STAT3 deletion blocked the transcription of target genes as expected. In contast, IL-6-induced gene expression was observed in STAT3$^{\Delta 372-387}$-expressing cells, albeit to a reduced magnitude compared with wild-type STAT3-expressing cells. These data suggest that this mutant retains transcriptional activity while abolishing the interaction with LRPPRC.

(E) The indicated cell lines were treated with IL-6 for 16 h and the expression of indicated STAT3-target genes determined. Data are mean fold gene induction relative to untreated for three independent experiments.
(F and G) A549 (F) or H1299 (G) lung adenocarcinoma cell lines with targeted deletion in STAT3, LRPPRC, or SLIRP or expression of the STAT3$\Delta^{372-387}$ mutant was injected into the flank of NSG mice and tumor volume monitored over time (n = 8 per group).
(H) Box and whiskers with paired, directional dot plot of SLIRP-STAT3 complex to nuclei ratio in matched healthy and tumor tissue from patients with lung adenocarcinoma ($p < 0.0001$, two-sided t test).
(I) Schematic overview of the proposed mechanism of mitochondrial STAT3 activity.
See related content in Figure S8.

STAT3, LRPPRC, or SLIRP loss delays tumor growth

Aberrant STAT3 signaling is a potent driver of tumorigenesis,[1] and the mitochondrial pool of STAT3 is required for transformation by RAS oncogenes.[4,6] To determine whether loss of the SLIRP-LRPPRC complex phenocopies the impact of STAT3 loss on tumorigenesis, KRAS mutant human lung adenocarcinoma (A549 and NCI-1299) cell lines with targeted deficiencies in *STAT3*, *SLIRP*, or *LRPPRC* were generated (Figures S4A and S4B) and transplanted into the flanks of immunocompromised NOD.Cg-Prkdc^{scid} Il2rg^{tm1Wjl}/SzJ/Arc (NSG) mice. As expected, the loss of STAT3 significantly delayed tumor growth (Figures 4E and 4F). The delay in tumor growth was phenocopied by the loss of SLIRP expression (Figures 4F and 4G), and the partial depletion of LRPPRC resulted in significantly delayed tumor growth (Figure 4G). However, it remained possible that altered tumorigenesis was due to a STAT3-, LRPPRC-, or SLIRP-dependent mechanism that was independent of their interaction. Therefore, we injected H1299-STAT3$^{\Delta 372–387}$ mutant cells into the flanks of NSG mice and observed a significant delay in tumor growth, which was greater than that observed in *STAT3*$^{-/-}$ and *LRPPRC*$^{+/-}$ H1299 cells, confirming the significance of this complex *in vivo* (Figure 4G). To determine whether the abundance of the STAT3-LRPPRC-SLIRP complex is elevated in patients with lung cancer, we performed PLA on tissue microarrays of early-stage resected lung adenocarcinoma specimens containing tumor and matched healthy tissue cores.[34] A significant increase in the abundance of this complex in tumor compared with matched healthy sections was observed (Figures 4H and S9A). Analysis of complex abundance in patients harboring *KRAS* or *EGFR* mutations revealed that while there is a significant increase in this complex in tumor compared with healthy tissue, there is no significant difference correlated to oncogenic mutation (Figure S9B), suggesting that the impact on tumor growth by targeting this complex will not be restricted to KRAS mutant patients.

DISCUSSION

Metabolic adaptation has been extensively described in cancer[35] and is emerging as a key regulator of immune function.[36] However, metabolic adaptation is not restricted to diseased cells. Rather, it is a requirement for any cell that needs to sacrifice efficient ATP production for the biomolecules required for proliferation. The discovery of a mitochondrial pool of STAT3 opened a non-canonical aspect of STAT3 biology, enabling direct metabolic control independent from a requirement on its nuclear transcription factor activity. Indeed, mitochondrial STAT3 has been reported in both healthy and diseased tissue,[37] but the most pronounced metabolic impacts have been reported in cancer[4] and immunity.[14]

The mechanism of mitochondrial STAT3 activity has been proposed to be dictated by a direct interaction with complex I of the ETC[5] and with the mPTP[11]; however, this is hard to reconcile with the relative deficit of STAT3 compared with ETC and mPTP proteins.[12] Nonetheless, we hypothesized that the mitochondrial activity of STAT3 would be dictated by protein-STAT3 interaction in a complex enabling a feedforward loop. This report describes one such mechanism—the interaction between STAT3, LRPPRC, and SLIRP. The LRPPRC-SLIRP complex regulates mtRNA polyadenylation, stability, and delivery to the mitochondrial ribosome. In the absence of STAT3 mature mtRNA stability, ribosome transport and translation are compromised. Each mitochondrially encoded mRNA is essential for the formation of the ETC. Therefore, any deficit in expression, stability, or translation, such as that driven by loss of STAT3, LRPPRC, or SLIRP, leads to inefficient oxidative phosphorylation. This magnifies the impact of a limited pool of STAT3 in the mitochondria (Figure 4I). We do not propose that STAT3, LRPPRC, and SLIRP expression is equivalent in the mitochondria, rather that STAT3 will interact with a proportion of the LRPPRC and SLIRP found in the mitochondria. Indeed, the magnitude of the impact of STAT3 loss on the activities of the LRPPRC-SLIRP complex is less dramatic than that observed following the loss of LRPPRC or SLIRP.[26,28] However, this substoichiometric relationship is biologically significant with respect to both mitochondrial RNA stability and translation and in the context of tumor formation.

STAT3 is an attractive therapeutic target in oncology. However, results from clinical trials of STAT3 inhibitors have been underwhelming.[38] These agents that target the nuclear activity of STAT3 are further confounded by the essentiality of STAT3 transcriptional potency for healthy biological function. While the mitochondrial activity of STAT3 is important in healthy tissue, the most dramatic impact of this facet of STAT3 biology is in tumorigenesis.[39] Our finding that the abundance of the STAT3-LRPPRC-SLIRP complex is significantly increased in lung tumor tissue compared with that observed in matched healthy tissue suggests that specifically targeting the mitochondrial activity of STAT3 will be an effective therapeutic approach while preserving the nuclear activity of STAT3 essential for healthy tissue.

Limitations of the study

Mitochondrial STAT3 represents a minor pool of total cellular STAT3. Therefore, the ability of a relatively small amount of STAT3 to influence more abundant mitochondrial protein complexes is likely to require a feedforward mechanism. The interaction of STAT3 with the LRPPRC-SLIRP complex, which is required for the stability and ribosomal translocation of mitochondrially encoded mRNA species, provides a plausible feedforward mechanism. However, the mitochondrial abundance of LRPPRC and SLIRP is greater than that of STAT3. Therefore, only a proportion of the LRPPRC-SLIRP heterotetrameric complexes will include STAT3. It is possible that STAT3 interacts with the LRPPRC-SLIRP complex in specific submitochondrial locations. Our data showing that the largest number of mitochondrial STAT3-interacting proteins are components of the mitochondrial ribosome are consistent with this hypothesis; however, this remains to be proven. We identify amino acids 372–387 of STAT3 as the LRPPRC-binding site. This resides in the DNA-binding domain of STAT3, and while we show transcriptional competency, additional work is required to understand whether this mutation alters STAT3 DNA-binding capacity and what the impact is on the entire STAT3-mediated transcriptome.

STAR★METHODS

Detailed methods are provided in the online version of this paper and include the following:

- KEY RESOURCES TABLE
- RESOURCE AVAILABILITY
  - Lead contact
  - Materials availability
  - Data and code availability
- EXPERIMENTAL MODEL AND SUBJECT DETAILS
  - Cell lines
  - Mouse xenograft models
- METHOD DETAILS
  - Stable cell line generation
  - Screening of cellulose-bound peptide Scans for STAT3-LRPPRC interaction site
  - Mitochondrial, nuclear, cytoplasmic and mitochondrial ribosomal isolation
  - Protein immunoprecipitation and expression analyses
  - Proteomics and chromatography
  - RNA isolation and gene expression analyses
  - Mitochondrial DNA (mtDNA) copy number
  - Mitochondrial RNA Ethynyl Uridine labeling
  - Mitochondrial polypeptide ^{35}S labeling
  - Seahorse assay
  - Multiplexed Poly(A)-Test RNA-sequencing
  - Proximity ligation assay
- QUANTIFICATION AND STATISTICAL ANALYSIS

SUPPLEMENTAL INFORMATION

Supplemental information can be found online at https://doi.org/10.1016/j.celrep.2023.113033.

ACKNOWLEDGMENTS

We thank the MHTP flow cytometry core, the Monash Medical Center Animal Facility, the Monash Micro Imaging Platform, Micromon, and the Bio21 Proteomics Facility for their expertise; M. Pagano, D. Levy, and J. StJohn for gifts of reagents; J. Balic and P. Hertzog for helpful discussions and editing; and G. Ballerin for image analysis support. This work is supported by the Operational Infrastructure Support Program by the Victorian Government of Australia. D.J. Gough is supported by a fellowship from the Victorian Cancer Agency (MCRF19033) and a grant from the Cancer Council Victoria (GNT1145028). D.J. Garama is supported by funding from the CASS Foundation. C.D.F. was supported by a Monash Research Training Scholarship. T.M.J. is an NHMRC Emerging Leader Fellow (2008341). Images were created in BioRender.

AUTHOR CONTRIBUTIONS

Study conception and design, D.J. Gough and D.J. Garama; experiments and data analysis, all authors; manuscript writing and editing, all authors.

DECLARATION OF INTERESTS

The authors declare no competing interests.

INCLUSION AND DIVERSITY

We support inclusive, diverse, and equitable conduct of research.

Received: January 6, 2022
Revised: June 16, 2023
Accepted: August 10, 2023
Published: September 12, 2023

REFERENCES

1. Huynh, J., Chand, A., Gough, D., and Ernst, M. (2019). Therapeutically exploiting STAT3 activity in cancer - using tissue repair as a road map. Nat. Rev. Cancer *19*, 82–96. https://doi.org/10.1038/s41568-018-0090-8.
2. Putoczki, T.L., Thiem, S., Loving, A., Busuttil, R.A., Wilson, N.J., Ziegler, P.K., Nguyen, P.M., Preaudet, A., Farid, R., Edwards, K.M., et al. (2013). Interleukin-11 is the dominant IL-6 family cytokine during gastrointestinal tumorigenesis and can be targeted therapeutically. Cancer Cell *24*, 257–271. https://doi.org/10.1016/j.ccr.2013.06.017.
3. Kralovics, R., Passamonti, F., Buser, A.S., Teo, S.S., Tiedt, R., Passweg, J.R., Tichelli, A., Cazzola, M., and Skoda, R.C. (2005). A gain-of-function mutation of JAK2 in myeloproliferative disorders. N. Engl. J. Med. *352*, 1779–1790. https://doi.org/10.1056/NEJMoa051113.
4. Gough, D.J., Corlett, A., Schlessinger, K., Wegrzyn, J., Larner, A.C., and Levy, D.E. (2009). Mitochondrial STAT3 supports Ras-dependent oncogenic transformation. Science *324*, 1713–1716, 324/5935/1713 [pii]. https://doi.org/10.1126/science.1171721.
5. Wegrzyn, J., Potla, R., Chwae, Y.J., Sepuri, N.B.V., Zhang, Q., Koeck, T., Derecka, M., Szczepanek, K., Szelag, M., Gornicka, A., et al. (2009). Function of mitochondrial Stat3 in cellular respiration. Science *323*, 793–797. https://doi.org/10.1126/science.1164551.
6. Gough, D.J., Marié, I.J., Lobry, C., Aifantis, I., and Levy, D.E. (2014). STAT3 supports experimental K-RasG12D-induced murine myeloproliferative neoplasms dependent on serine phosphorylation. Blood *124*, 2252–2261. https://doi.org/10.1182/blood-2013-02-484196.
7. Garama, D.J., Harris, T.J., White, C.L., Rossello, F.J., Abdul-Hay, M., Gough, D.J., and Levy, D.E. (2015). A Synthetic Lethal Interaction between Glutathione Synthesis and Mitochondrial Reactive Oxygen Species Provides a Tumor-Specific Vulnerability Dependent on STAT3. Mol. Cell Biol. *35*, 3646–3656. https://doi.org/10.1128/MCB.00541-15.
8. Mackenzie, G.G., Huang, L., Alston, N., Ouyang, N., Vrankova, K., Mattheolabakis, G., Constantinides, P.P., and Rigas, B. (2013). Targeting mitochondrial STAT3 with the novel phospho-valproic acid (MDC-1112) inhibits pancreatic cancer growth in mice. PLoS One *8*, e61532. https://doi.org/10.1371/journal.pone.0061532.
9. Zhou, L., and Too, H.P. (2011). Mitochondrial localized STAT3 is involved in NGF induced neurite outgrowth. PLoS One *6*, e21680. https://doi.org/10.1371/journal.pone.0021680.
10. Boengler, K., Hilfiker-Kleiner, D., Heusch, G., and Schulz, R. (2010). Inhibition of permeability transition pore opening by mitochondrial STAT3 and its role in myocardial ischemia/reperfusion. Basic Res. Cardiol. *105*, 771–785. https://doi.org/10.1007/s00395-010-0124-1.
11. Meier, J.A., Hyun, M., Cantwell, M., Raza, A., Mertens, C., Raje, V., Sisler, J., Tracy, E., Torres-Odio, S., Gispert, S., et al. (2017). Stress-induced dynamic regulation of mitochondrial STAT3 and its association with cyclophilin D reduce mitochondrial ROS production. Sci. Signal. *10*, eaag2588. https://doi.org/10.1126/scisignal.aag2588.
12. Phillips, D., Reilley, M.J., Aponte, A.M., Wang, G., Boja, E., Gucek, M., and Balaban, R.S. (2010). Stoichiometry of STAT3 and mitochondrial proteins: Implications for the regulation of oxidative phosphorylation by protein-protein interactions. J. Biol. Chem. *285*, 23532–23536, C110.152652 [pii]. https://doi.org/10.1074/jbc.C110.152652.
13. Betto, R.M., Diamante, L., Perrera, V., Audano, M., Rapelli, S., Lauria, A., Incarnato, D., Arboit, M., Pedretti, S., Rigoni, G., et al. (2021). Metabolic control of DNA methylation in naive pluripotent cells. Nat. Genet. *53*, 215–229. https://doi.org/10.1038/s41588-020-00770-2.
14. Balic, J.J., Albargy, H., Luu, K., Kirby, F.J., Jayasekara, W.S.N., Mansell, F., Garama, D.J., De Nardo, D., Baschuk, N., Louis, C., et al. (2020).

STAT3 Serine phosphorylation is required for TLR4 metabolic reprogramming and IL-1beta expression. Nat. Commun. *11*, 3816.

15. Shannon, P., Markiel, A., Ozier, O., Baliga, N.S., Wang, J.T., Ramage, D., Amin, N., Schwikowski, B., and Ideker, T. (2003). Cytoscape: a software environment for integrated models of biomolecular interaction networks. Genome Res. *13*, 2498–2504. https://doi.org/10.1101/gr.1239303.
16. Bindea, G., Mlecnik, B., Hackl, H., Charoentong, P., Tosolini, M., Kirilovsky, A., Fridman, W.H., Pagès, F., Trajanoski, Z., and Galon, J. (2009). ClueGO: a Cytoscape plug-in to decipher functionally grouped gene ontology and pathway annotation networks. Bioinformatics *25*, 1091–1093. https://doi.org/10.1093/bioinformatics/btp101.
17. Calvo, S.E., Clauser, K.R., and Mootha, V.K. (2016). MitoCarta2.0: an updated inventory of mammalian mitochondrial proteins. Nucleic Acids Res. *44*, D1251–D1257. https://doi.org/10.1093/nar/gkv1003.
18. Spåhr, H., Rozanska, A., Li, X., Atanassov, I., Lightowlers, R.N., Chrzanowska-Lightowlers, Z.M.A., Rackham, O., and Larsson, N.G. (2016). SLIRP stabilizes LRPPRC via an RRM-PPR protein interface. Nucleic Acids Res. *44*, 6868–6882. https://doi.org/10.1093/nar/gkw575.
19. Sasarman, F., Brunel-Guitton, C., Antonicka, H., Wai, T., and Shoubridge, E.A.; LSFC Consortium (2010). LRPPRC and SLIRP interact in a ribonucleoprotein complex that regulates posttranscriptional gene expression in mitochondria. Mol. Biol. Cell *21*, 1315–1323. https://doi.org/10.1091/mbc.E10-01-0047.
20. Mili, S., and Piñol-Roma, S. (2003). LRP130, a pentatricopeptide motif protein with a noncanonical RNA-binding domain, is bound in vivo to mitochondrial and nuclear RNAs. Mol. Cell Biol. *23*, 4972–4982.
21. Hatchell, E.C., Colley, S.M., Beveridge, D.J., Epis, M.R., Stuart, L.M., Giles, K.M., Redfern, A.D., Miles, L.E.C., Barker, A., MacDonald, L.M., et al. (2006). SLIRP, a small SRA binding protein, is a nuclear receptor corepressor. Mol. Cell *22*, 657–668. https://doi.org/10.1016/j.molcel.2006.05.024.
22. Balic, J.J., Garama, D.J., Saad, M.I., Yu, L., West, A.C., West, A.J., Livis, T., Bhathal, P.S., Gough, D.J., and Jenkins, B.J. (2019). Serine-Phosphorylated STAT3 Promotes Tumorigenesis via Modulation of RNA Polymerase Transcriptional Activity. Cancer Res. *79*, 5272–5287. https://doi.org/10.1158/0008-5472.CAN-19-0974.
23. Kukat, C., and Larsson, N.G. (2013). mtDNA makes a U-turn for the mitochondrial nucleoid. Trends Cell Biol. *23*, 457–463. https://doi.org/10.1016/j.tcb.2013.04.009.
24. Slomovic, S., and Schuster, G. (2008). Stable PNPase RNAi silencing: its effect on the processing and adenylation of human mitochondrial RNA. RNA *14*, 310–323. https://doi.org/10.1261/rna.697308.
25. Wydro, M., Bobrowicz, A., Temperley, R.J., Lightowlers, R.N., and Chrzanowska-Lightowlers, Z.M. (2010). Targeting of the cytosolic poly(A) binding protein PABPC1 to mitochondria causes mitochondrial translation inhibition. Nucleic Acids Res. *38*, 3732–3742. https://doi.org/10.1093/nar/gkq068.
26. Ruzzenente, B., Metodiev, M.D., Wredenberg, A., Bratic, A., Park, C.B., Cámara, Y., Milenkovic, D., Zickermann, V., Wibom, R., Hultenby, K., et al. (2012). LRPPRC is necessary for polyadenylation and coordination of translation of mitochondrial mRNAs. EMBO J. *31*, 443–456. https://doi.org/10.1038/emboj.2011.392.
27. Chujo, T., Ohira, T., Sakaguchi, Y., Goshima, N., Nomura, N., Nagao, A., and Suzuki, T. (2012). LRPPRC/SLIRP suppresses PNPase-mediated mRNA decay and promotes polyadenylation in human mitochondria. Nucleic Acids Res. *40*, 8033–8047. https://doi.org/10.1093/nar/gks506.
28. Lagouge, M., Mourier, A., Lee, H.J., Spåhr, H., Wai, T., Kukat, C., Silva Ramos, E., Motori, E., Busch, J.D., Siira, S., et al. (2015). SLIRP Regulates the Rate of Mitochondrial Protein Synthesis and Protects LRPPRC from Degradation. PLoS Genet. *11*, e1005423. https://doi.org/10.1371/journal.pgen.1005423.
29. DepMap, B. (2020). DepMap 20Q2 Public. https://figshare.com/articles/dataset/DepMap_20Q2_Public/12280541.
30. Dufourt, J., Bontonou, G., Chartier, A., Jahan, C., Meunier, A.C., Pierson, S., Harrison, P.F., Papin, C., Beilharz, T.H., and Simonelig, M. (2017). piRNAs and Aubergine cooperate with Wispy poly(A) polymerase to stabilize mRNAs in the germ plasm. Nat. Commun. *8*, 1305. https://doi.org/10.1038/s41467-017-01431-5.
31. Macias, E., Rao, D., Carbajal, S., Kiguchi, K., and DiGiovanni, J. (2014). Stat3 binds to mtDNA and regulates mitochondrial gene expression in keratinocytes. J. Invest. Dermatol. *134*, 1971–1980. https://doi.org/10.1038/jid.2014.68.
32. Vassilev, A.O., Lorenz, D.R., Tibbles, H.E., and Uckun, F.M. (2002). Role of the leukemia-associated transcription factor STAT3 in platelet physiology. Leuk. Lymphoma *43*, 1461–1467. https://doi.org/10.1080/1042819022386716.
33. D'Souza, A.R., and Minczuk, M. (2018). Mitochondrial transcription and translation: overview. Essays Biochem. *62*, 309–320. https://doi.org/10.1042/EBC20170102.
34. Cooper, W.A., Tran, T., Vilain, R.E., Madore, J., Selinger, C.I., Kohonen-Corish, M., Yip, P., Yu, B., O'Toole, S.A., McCaughan, B.C., et al. (2015). PD-L1 expression is a favorable prognostic factor in early stage non-small cell carcinoma. Lung Cancer *89*, 181–188. https://doi.org/10.1016/j.lungcan.2015.05.007.
35. Vander Heiden, M.G., and DeBerardinis, R.J. (2017). Understanding the Intersections between Metabolism and Cancer Biology. Cell *168*, 657–669. https://doi.org/10.1016/j.cell.2016.12.039.
36. Zasłona, Z., and O'Neill, L.A.J. (2020). Cytokine-like Roles for Metabolites in Immunity. Mol. Cell *78*, 814–823. https://doi.org/10.1016/j.molcel.2020.04.002.
37. Garama, D.J., White, C.L., Balic, J.J., and Gough, D.J. (2016). Mitochondrial STAT3: Powering up a potent factor. Cytokine *87*, 20–25. https://doi.org/10.1016/j.cyto.2016.05.019.
38. Beebe, J.D., Liu, J.Y., and Zhang, J.T. (2018). Two decades of research in discovery of anticancer drugs targeting STAT3, how close are we? Pharmacol. Ther. *191*, 74–91. https://doi.org/10.1016/j.pharmthera.2018.06.006.
39. Demaria, M., Camporeale, A., and Poli, V. (2014). STAT3 and metabolism: how many ways to use a single molecule? International journal of cancer. Int. J. Cancer *135*, 1997–2003. https://doi.org/10.1002/ijc.28767.
40. O'Brien, T.W. (1971). The general occurrence of 55 S ribosomes in mammalian liver mitochondria. J. Biol. Chem. *246*, 3409–3417.
41. Lee, W., Johnson, J., Gough, D.J., Donoghue, J., Cagnone, G.L.M., Vaghjiani, V., Brown, K.A., Johns, T.G., and St John, J.C. (2015). Mitochondrial DNA copy number is regulated by DNA methylation and demethylation of POLGA in stem and cancer cells and their differentiated progeny. Cell Death Dis. *6*, e1664. https://doi.org/10.1038/cddis.2015.34.
42. López-Cano, M., Fernández-Dueñas, V., and Ciruela, F. (2019). Proximity Ligation Assay Image Analysis Protocol: Addressing Receptor-Receptor Interactions. Methods Mol. Biol., 41–50. https://doi.org/10.1007/978-1-4939-9686-5_3.

STAR★METHODS

KEY RESOURCES TABLE

REAGENT or RESOURCE	SOURCE	IDENTIFIER
Antibodies		
Rabbit polyclonal anti-LRPPRC	Abcam	205022
Mouse monoclonal anti-STAT3	Cell Signaling Technology	9139; RRID:AB_331757
Rabbit polyclonal anti-SLIRP	Abcam	51523; RRID:AB_2066704
Rabbit polyclonal anti-VDAC	Cell Signaling Techology	4661; RRID:AB_10557420
Rabbit polyclonal anti-MRPL37	Proteintech	15190-1-AP; RRID:AB_2146040
Rabbit polyclonal anti-MRPS35	Proteintech	16457-1-AP; RRID:AB_2146521
Rabbit monoclonal anti-BiP (C50B12)	Cell Signaling Techology	3177; RRID:AB_2119845
Mouse monoclonal anti-Lamin A/C (4C11)	Cell Signaling Techology	4777; RRID:AB_10545756
Mouse monoclonal anti-FLAG (M2)	Merck	F1804; RRID:AB_262044
Donkey anti-mouse IRDye 680LT	LiCOR	926–68022
Donkey anti-rabbit IRDye 800CW	LiCOR	926–32213
Bacterial and virus strains		
E. Coli strain Top10	Thermo Fisher	C404010
E. Coli strain Stbl3	Thermo Fisher	C737303
Biological samples		
Human LUAD patient samples and adjacent normal tissue	W.A Cooper and M.R.J Kohonen-Corish	Cooper et al.[34]
Chemicals, peptides, and recombinant proteins		
Celluspot cellulose array	Intavis	93.010
Dynabeads Protein A	Thermo Fisher	10001D
Anti-FLAG M2 magnetic beads	Merck	M8823
Strep-Tactin XT Sepharose resin	Merck	GE29401324
Dynabeads® MyOne Streptavidin T1	Thermo Fisher	65602
Critical commercial assays		
Transcriptor High Fidelity cDNA systhesis kit	Merck	5091284001
Click-iT Nascent RNA Capture Kit	Thermo Fisher	C10365
Expre35S35S Protein Labeling Mix	Perkin Elmer	NEG072002MC
MitoStress Test Kit	Agilent	103010–100
Duolink® *In Situ* Green Kit (Mouse/Rabbit)	Merck	DUO92014
Deposited data		
Mass spectrometry data	This paper	ProteomeXchange accession: PXD044281
mPAT Sequencing data	This paper	FigShare https://doi.org/10.26180/23849112
Experimental models: Cell lines		
A549	ATCC	CCL-185
MKN-28	JCRB	JCRB0253
NCI-H1299	ATCC	CRL-5803
Lenti-X 293T	Takara	632180
HRasV12 transformed MEFs	Gough et al.[4]	N/A
Experimental models: Organisms/strains		
NOD.Cg-Prkdc^{scid} Il2rg^{tm1Wjl}/SzJ/Arc mice	Animal Resources Center, Canning Vale, Australia	N/A

(*Continued on next page*)

Continued

REAGENT or RESOURCE	SOURCE	IDENTIFIER
Oligonucleotides		
STAT3 sgRNA1: ACTGCTGGTCAATCTCTCCC	Merck	N/A
STAT3 sgRNA2: AGATTGCCCGGATTGTGGCC	Merck	N/A
LRPPRC sgRNA1: TTGGCAAAAGCCTTAATGAAGG	Merck	N/A
LRPPRC sgRNA2: AATGGCATACAGCCTGGCTGGG	Merck	N/A
SLIRP sgRNA1: GTAAAATGCACCTTCTGACA	Merck	N/A
SLIRP sgRNA2: GAGAAGAATTCCTTGGACTG	Merck	N/A
qRT-PCR and mPAT primer sequences are listed in Tables S2 and S3 respectively		N/A
Software and algorithms		
GraphPad Prism V10	GraphPad	https://www.graphpad.com/features
Fiji V1.0	NIH	https://ImageJ.net/software/fiji/downloads
Cytoscape plugin ClueGO	Shannon et al. and Bindea et al.[15,16]	https://cytoscape.org
PyMOL Molecular Graphics System, Version 2.4	Schrödinger	https://pymol.org/2/
Proteome Discoverer V2.1	Thermo Fisher	OPTON-31099

RESOURCE AVAILABILITY

Lead contact

Further information and requests for resources and reagents should be directed to and will be fulfilled by the Lead Contact, Daniel Gough (Daniel.gough@hudson.org.au).

Materials availability

All unique reagents generated in this study are available from the lead contact with a completed Materials Transfer Agreement.

Data and code availability

Proteomics data have been deposited at the ProteomeXchange, mPAT-sequencing data are publicly available at FigShare as of the date of publication. Accession numbers are listed in the key resources table. Any additional information required to reanalyze the data reported in this paper is available from the lead contact upon request.

This paper does not report original code.

EXPERIMENTAL MODEL AND SUBJECT DETAILS

Cell lines

Human cancer cell lines A549, MKN-28 and NCI-H1299 were purchased from the American Type Culture Collection or the Japanese Collection of Research Bioresources Cell Bank and maintained in Advanced Roswell Park Memorial Institute (RPMI) 1640 media (Gibco) supplemented with 1% fetal calf serum (FCS; Bovogen) and 2mM L-Glutamine (Gibco). Cell line identification was authenticated by short tandem repeat profiling (PowerPlex HS16 System KIT, Promega) prior to study commencement, and cells were passaged during experiments for under 3 months at a time between freeze/thaw cycles. Lenti-X 293T cells (Takara) and HRasV12 transformed MEFs[4] were cultured in Dulbecco's modified Eagle's medium supplemented with 10% FCS, 1mM sodium pyruvate (Gibco) and 2mM L-glutamine. Cells were routinely tested for mycoplasma contamination (MycoAlert PLUS Mycoplasma Detection Kit, Lonza). Cells were cultured at 37°C supplemented with 5% CO_2 in a humidified chamber.

The A549 Rho0 cell line was generated by continuous culture in advanced RPMI supplemented with 1% fetal bovine serum (FBS; Bovogen) and 2mM L-Glutamine (Gibco), Ethidium bromide (50 ng/mL), pyruvate (1 mM) and uridine (50 μg/mL) until cells lacked any electron transport chain activity as measured by Seahorse assay.

Mouse xenograft models

All animals were housed under specific pathogen–free (SPF) conditions, and experiments were approved by the Monash Medical Center "A" Animal Ethics Committee (ethics number MMCA/2017/01). For xenograft studies, cells were collected from sub-confluent cell culture plates, washed twice with PBS and resuspended in 50% (v/v) PBS diluted Matrigel (Corning). 1×10^6 cells were subcutaneously injected into the right back flank of 6–8 week old, male and female, NOD.Cg-Prkdc^{scid} Il2rg^{tm1Wjl}/SzJ/Arc (NSG) mice (Animal Resources Center, Canning Vale, Australia), and tumor size was measured three times per week using electronic calipers and tumor volume calculated using the formula (W^2xL)/2 = Vmm[3]).

METHOD DETAILS

Stable cell line generation

Self-complementary oligonucleotides (Sigma-Aldrich) used as single-guided (sg)RNA sequences targeting human *STAT3*, LRPPRC or SLIRP were ligated into the LentiCRISPRv2 construct (Addgene plasmid#52961). sgRNA sequences are listed in the key resources table. Lentivirus was produced by transfecting vectors into Lenti-X/H293T (Clonetech) cells with LentiCRISPR:psPAX2:pMD2.G at a ratio of 4:3:1. Virus was harvested 48 h after transfection, filtered, and used to infect cell cultures containing 5 μg/mL polybrene. Infected cells were selected with puromycin, and cells infected with nontarget control sgRNA vector were used as negative controls.

STAT3 or mitochondrially restricted STAT3 (MTS)[4] cDNA was PCR amplified and cloned into the NheI and XhoI sites of pCDNA3.1-NSFII (gift from Michele Pagano, NYU) fusing STAT3 cDNA with Streptactin and FLAG tags. Tagged STAT3 cDNA was subcloned into the lentiviral pLVX-IRES-mCherry vector (Clonetech). To clone putative STAT3-LRPPRC binding mutants, gene block DNA was ordered from Integrated DNA Technologies with each 15 amino acid regions deleted and cloned into the pLVX-IRES-mCherry vector containing a wild-type STAT3 cDNA using Gibson Cloning (New England Biolabs). Sequences of each clone was verified by sanger sequencing (MicroMon). STAT3 reconstituted cells were generated by transducing $STAT3^{-/-}$ cells with virus generated as above. After viral transduction cells were sorted and titrated for mCherry by flow cytometry to ensure equivalent STAT3 expression levels, and to select for cell populations that approximated the endogenous expression of STAT3 in the parental cell line. pLVX EV (empty vector) denotes the parental vector used as controls. All vectors were sequenced for validation. Cloning primers are available upon request.

Screening of cellulose-bound peptide Scans for STAT3-LRPPRC interaction site

15 amino acid peptides tiling the full length of wild-type STAT3 and overlapping by 4 amino acids were designed. Peptides were synthesized and C-terminally linked to a cellulose membrane (Intavis, part number 93.010). Dry membranes were incubated in odyssey blocking buffer (Li-COR) for 1 h at room temperature. Cell lysates from $STAT3^{-/-}$ or $SLIRP^{-/-}$ H1299 cells were diluted to 1mg in 500μL and added to blocked peptide array. Arrays were incubated in cell lysate for 4 h at 4°C, washed 3 times in TBS+1%Tween 20, and primary antibody added (Rabbit anti-LRPPRC, abcam #ab205022) at a 1:1000 dilution overnight at 4°C. Arrays were washed 3 times in TBS+1%Tween 20 and incubated in IRDye fluorescent secondary antibodies (1:10,000 dilution) and imaged using an Odyssey CLx imaging system (LI-COR Biosciences). The grid function in the analysis package was used for densitometry and biding intensity of each spot determined, background subtraction performed, and data presented as the mean intensity +/− SD for three independent experiments.

Mitochondrial, nuclear, cytoplasmic and mitochondrial ribosomal isolation

Mitochondrial, nuclear and S100 cytoplasmic fractions were isolated as described previously.[4]

Mitochondrial ribosomes were isolated as previously described[40] with minor modifications. Mitochondria were resuspended in 1 mL of Tris-magnesium-potassium buffer (10 mM Tris-HCl; pH 7.4, 10 mM magnesium acetate, 100 mM Potassium chloride) and lysed by addition of 100 μL of 10% Triton X-100 on ice for 20 min. Lysed mitochondria were centrifuged at 17,000g for 10 min. Mitochondrial supernatant was layered on top of 10 mL of sucrose cushion buffer (34% w/v sucrose in Tris-magnesium-potassium buffer with 1% Triton X-100) and subjected to centrifugation at 105,000g for 14 h at 4°C using a V100X Preparative Ultracentrifuge, VWR (Beckman-Coulter, Life Sciences) equipped with P40ST swinging bucket rotor. The supernatant was removed leaving the pelleted 55S ribosome for subsequent analysis.

Protein immunoprecipitation and expression analyses

Isolated mitochondria (2 mg) lysed in whole cell lysis buffer (50 mM Tris-HCl; pH 7.4, 150 mM Sodium chloride, 1 mM EGTA, 0.5% Triton X-100) supplemented with protease inhibitor cocktail (EDTA-free, Thermo Scientific, #78415) and DTT (1mM) were pre-cleared with Dynabeads Protein A (Life Technologies, 10001D) at 4°C for 15 min. A sample of pre-cleared supernatant was retained as the input sample and specific antibody against bait protein (1–10 μg) added to remaining sample and incubated at 4°C with rotation. Protein complexes were collected on Dynabeads Protein A (15 μL) and washed three times with whole cell lysis buffer. Protein was eluted in SDS loading buffer and boiled for 5 min before resolution by SDS-PAGE. Protein expression was analyzed by Western blot. The following antibodies were used: STAT3 Mouse Monoclonal (Cell Signaling Technology, #9139S (124 H6)), LRPPRC Rabbit Polyclonal (Abcam, #ab205022), SLIRP Rabbit Polyclonal (Abcam, #ab51523), VDAC Rabbit Monoclonal (Cell Signaling Technology, #4661S), MRPL37 Rabbit Polyclonal (Proteintech, #15190-1-AP), MRPS35 Rabbit Polyclonal (Proteintech, #16457-1-AP), BiP, LaminA/C. Images of membranes were obtained using IRDye fluorescent secondary antibodies and an Odyssey CLx imaging system (LI-COR Biosciences).

Proteomics and chromatography

Following immunoprecipitation protein-bead complexes were washed 5 times with wash buffer (Tris-HCl (50 mM, pH 7.4), NaCl (150 mM), EGTA (1 mM) and Triton X-100 (0.5%), followed by 3 washes in 50mM triethylammonium bicarbonate buffer (TEAB; Sigma Aldrich). Protein-bead complexes were digested overnight in 30μL of 50mM TEAB containing 300ng of sequencing grade trypsin (ThermoFisher), 1mM Tris(2-carboxyethyl)phosphine (TCEP) (ThermoFisher) and 1mM TFA at 37°C.

Digested peptides were exsiccated and prior to analysis reconstituted in loading buffer (0.1% formic acid/2% acetonitrile/water). 4–6 μl aliquots of peptide mixture was analyzed by nano-LC-MS/MS. LC-MS/MS was performed using a Fusion Lumos Orbitrap mass spectrometer (Thermo Fisher, USA) in positive-ionization mode, with the spray voltage set at 1.9 kV and the ion transfer capillary temperature at 275°C. Tryptic peptides were injected into an enrichment column (DinoexC18,100 Å, 75μm × 2cm) at an isocratic flow of 5 μL/min of 2% v/v acetonitrile containing 0.1% v/v formic acid for 6min, before the enrichment column was switched in-line with the analytical column (Dinoex-C18, 100Å, 75μm × 50cm). The eluents were 0.1% v/v formic acid (solvent A) in water and 100% v/v acetonitrile in 0.1% v/v formic acid (solvent B). The flow gradient was (i) 0-6 min at 3% B; (ii) 6-35min, 3–22% B; (iii) 35-40min, 22–40% B; (iv) 45-50min, 40–80% B; (v) 50- 55min, 80-80% B; (vi) 55-56min 85-3% and equilibrated at 3% B for 10min before injecting the next sample. Full MS1 spectra were acquired in a positive mode at 120,000 resolution at m/z 200, with an AGC target of 5e5. The ''top speed'' acquisition mode (cycle time: 3sec) on the most intense precursor ion was used, whereby ions with charge states of 2–5 were isolated using an isolation window of 1.2m/z and fragmented with using HCD with a stepped collision energy of 30 ± 5%. Fragment ion spectra were acquired in Orbitrap at 15,000 resolution at m/z 200. Dynamic exclusion was 30sec.

Data were analyzed using Proteome Discoverer (Thermo Scientific version 2.1) with the Mascot search engine against the SWISSPROT Mus Musculus and Homo Sapiens databases (build June 2015). Search parameters were set at precursor mass tolerance of 20 ppm and fragment mass tolerance of 0.5 Da. Trypsin with a maximum of two missed cleavages was used as the cleavage enzyme, and oxidized methionine was included as variable modification.

RNA isolation and gene expression analyses

Total RNA was isolated from cell lines, isolated mitochondria or mitochondrial ribosomal fractions using TRIzol or TRIzol LS solution for liquid samples (Invitrogen), followed by DNase treatment (Qiagen). RNA was transcribed using the Transcriptor High Fidelity cDNA Synthesis Kit (Roche) and random hexamers or poly(d-T) primers as indicated. Quantitative real-time PCR (qPCR) was performed using the QuantStudio6 RT-PCR System. Primer sequences for the following genes are detailed in Table S2:

MT-ND1, *MT-ND6*, *MT-ND4L*, *MT-ND4*, *MT-COX1*, *MT-COX2*, *MT-COX3*, *MT-ATP6*, *MT-CYTB*, *MT-RNR1*, *MT-RNR2*, *MT-COX3/ND3* Junction, *B2M* and *ACTB*.

Mitochondrial DNA (mtDNA) copy number

Genomic DNA was isolated from cell pellets using the ISOLATE II Genomic DNA Kit (Bioline), and further subjected to RNAse A treatment (Qiagen). qPCR was performed on a QuantStudio6 RT-PCR System (Thermo-Fischer) using power-SYBR green master mix (Thermo-Fischer). Three pairs of primers - two specific for mitochondrial genome *MT-COX1* and *MT-RNR2* and another pair specific for the nuclear genome (*B2M*) - were designed for the quantification of mtDNA copy number. The ratio of mtDNA copy number to the amount of nuclear DNA was calculated based on previously described methodology.[41]

Mitochondrial RNA Ethynyl Uridine labeling

Three EU labeling protocols were performed all using the Click-iT Nascent RNA Capture Kit, Molecular Probes by Life Technologies (#C10365) following manufacturer's protocols for RNA biotinylation, capture and precipitation. Specific EU labeling protocols follow:

Pulse labeling to determine mitochondrial transcription kinetics

Mitochondria were isolated from A549 STAT3 wild-type and knockout cell lines and 1 mg of intact mitochondria were resuspended in 1 mL of transcription buffer (50 mM Tris; pH 7.4, 25 mM Sucrose, 75 mM Sorbitol, 100 mM Potassium chloride, 10 mM Dipotassium hydrogen phosphate, 50 μM EDTA, 5 mM Magnesium chloride, 10 mM Glutamate 10 mM, 2.5 mM Diethyl malate, 1 mg/mL Bovine serum albumin, 1 mM ADP) supplemented with 0.5 mM final concentration of EU (Component A, Click-iT Nascent RNA Capture Kit, Molecular Probes by Life Technologies, #C10365) for 1 h at 37°C. Mitochondria were collected by centrifugation (10,000g, 5 min at 4°C) and RNA isolated using Trizol (Invitrogen, Catalog numbers 15596026 and 15596018) according to manufacturer's instructions. 1 μg of RNA was biotinylated using the Click-iT Nascent RNA Capture Kit (Molecular Probes by Life Technologies), captured on Dynabeads MyOne Streptavidin T1 beads and used as a template for cDNA synthesis with Random Hexamer primers and quantitative Real-Time PCR performed as described above. Relative fold change was expressed relative to that observed in $STAT3^{+/+}$ cells in at least three independent experiments. ***Ethynyl Uridine (EU) labeling of cells to determine mitochondrial RNA stability***. A549 STAT3 wild-type and knockout cells were grown in 6-well plates to 70% confluency and pulsed with EU (0.5 mM final concentration) for 6 h. Cells were washed in media 3 times and incubated in fresh media for 16 h at 37°C and 5% CO_2. Cells were washed, RNA extracted, biotinylated, captured, reverse transcribed and subjected to quantitative real-time PCR as described previously. The expression of each gene was normalized against the nuclear encoded house-keeping gene *ACTB* and expressed as the relative fold change of each mitochondrial gene in $STAT3^{+/+}$ with respect to $STAT3^{-/-}$ as determined by ΔΔCt method in at least three independent experiments.

Ethynyl Uridine (EU) labeling of RNA in mitochondrial ribosomes

Mitochondria were isolated, quantified and 1mg labeled with EU as described above. Mitochondrial ribosomes were isolated as described above and the RNA in the ribosomal pellet was extracted using Trizol reagent (Invitrogen, Catalog numbers 15596026 and 15596018). RNA quantitation, biotynlation, reverse transcription and quantitation by qRT-PCR as described above. Relative fold change was expressed as the ratio of the absolute quantities of gene of interest between $STAT3^{+/+}$ and $STAT3^{-/-}$ in at least three independent experiments.

Mitochondrial polypeptide ^{35}S labeling

Cells were cultured to ~80% confluence, washed twice and then incubated in pre-warmed Methionine and Cysteine free RPMI at 37°C for 30 min. Emetine was added to a final concentration of 100 μg/mL to block cytoplasmic ribosomes and dialyzed FBS to a final concentration of 10% and cells were incubated at 37°C for 10 min ^{35}S labeled Methionine and Cysteine was added (0.05mCi, NEG072002MC PerkinElmer) and incubated at 37°C for 2 h. Cells were washed and lysed in 150mM NaCl, 50mM Tris (pH 7.4), 1mM EDTA, 0.5% Triton X-100, protease inhibitor cocktail (Sigma Aldrich), 1mM NaF, 1mM β-glycerophosphate, 1mM Na_3VO_4 and 1mM DTT and quantified. Equivalent protein was added to Laemmle loading dye and incubated at room temperature for 30 min prior to vortexing for 1 min and resolving through 4–12.5% SDS-PAGE. Gels were fixed in 30% Methanol, 10% acetic acid and 60% ddH_2O overnight and dehydrated in 50% ethanol, 50% ddH_2O for 30 min before drying at 80°C for 2 h on vacuum gel dryer. Gels were expose to phosphor-screen for a minimum of 3 days before imaging on a typhpoon multimode imaging system.

Seahorse assay

Cells were plated at 10^4 cells/well on an XFp plate (Agilent) in advanced RPMI supplemented with 1%FCS, glutamine and non-essential amino acids. A utility plate containing the injector ports and probes was filled with calibrant solution (200 μL/well) and placed in a CO2-free incubator at 37°C overnight. On the day of experiment, cells were washed twice in seahorse RPMI media and replaced with XF assay media pH 7.4 supplemented with 10mM glucose, 1 mM pyruvate and 2 mM glutamine (Sigma). The cell culture plate was placed in a CO2-free incubator for 60 min. Oligomycin (ATPase inhibitor, 1 μM), FCCP (1.5 μM) and Rotenone/Antimycin A (1 μM each) were added to the appropriate ports of the utility plate and a standard MitoStress test protocol used according to manufacturer's protocols.

Multiplexed Poly(A)-Test RNA-sequencing

Mitochondrial mRNA poly(A) tail lengths were determined as previously published.[30] adenylated 3′ termini were extended with Klenow fragment of DNA polymerase 1 in the presence of an oligo dT-anchor-oligo and reverse transcribed using a primer annealed to the anchor sequence. The cDNA of genes of interest was PCR amplified in a nested PCR reaction with first gene specific primers, then Illumina compatible bridging primers, for next generation sequencing on an Ilumina MiSeq platform. Gene specific primer sequences are detailed in Table S3.

Proximity ligation assay

For PLA on cell culture cells were seeded on coverslips in 24 well plates and incubated with mitotracker Red (ThermoFischer, M7512) at a final concentration of 100nM for 30 min. Cells were washed in PBS and fixed in 4% formaldehyde/PBS and permeabilized with 100% ice-cold methanol. PLA was carried out using the Duolink *In Situ* Green Kit (Mouse/Rabbit) (Sigma; DUO92014). Antibody combinations included STAT3 (Cell Signaling Technology; 9139) with either LRPPRC (Abcam; ab97505) or SLIRP (Abcam; ab51523). STAT3-deficient cells were employed to determine the background of the assay. Images were acquired on a Nikon C1 confocal microscope. For PLA on tissue microarrays sections were dewaxed, rehydrated, then boiled in a pressure cooker for 20 min in 0.01M citrate buffer (pH 6.0) for antigen retrieval, blocking, antibody incubation and PLA reaction were performed as for cultured cells with the addition autofluorescence quenching using the TrueView Autofluorescence Quenching Kit (Vector Laboratories). Slides were scanned on a VS.120 fluorescent slide scanner (Olympus). Analysis and quantification were performed using FiJi software.[42]

QUANTIFICATION AND STATISTICAL ANALYSIS

All statistical analyses were performed using GraphPad Prism V7.0 software or R package. All experiments were performed with a minimum of three independent biological replicates. Statistical significance ($p < 0.05$) between the means of two groups was determined using Student t-tests or Mann-Whitney U tests, and for matched datasets involved Wilcoxon signed-rank tests. Statistical comparisons of the means of multiple groups were determined using one-way ANOVA.